Physics and Chemistry of the Earth 45–46 (2012) 50–64

Contents lists available at SciVerse ScienceDirect

Physics and Chemistry of the Earth

journal homepage: www.elsevier.com/locate/pce

Long-range volcanic ash transport and fallout during the 2008 eruption of Chaitén volcano, Chile

Adam J. Durant [a,b,c,*], Gustavo Villarosa [d], William I. Rose [b], Pierre Delmelle [e], Alfred J. Prata [a], José G. Viramonte [f]

[a] Norwegian Institute for Air Research, P.O. Box 100, NO-2027 Kjeller, Norway
[b] Geological and Mining Engineering and Sciences, Michigan Technological University, USA
[c] Centre for Atmospheric Science, Department of Chemistry, University of Cambridge, Lensfield Road, Cambridge, CB2 1EW, UK
[d] INIBIOMA, CONICET – Universidad Nacional del Comahue, Quintral 1250, 8400 Bariloche, Río Negro, Argentina
[e] Environment Department, University of York, Heslington, York, UK
[f] Universidad Nacional de Salta – CONICET – INENCO-GEONORTE, Av. Bolivia 5150, 4400 Salta, Argentina

ARTICLE INFO

Article history:
Available online 17 September 2011

Keywords:
Volcanic ash
Chaitén
Fallout
Satellite remote sensing
Aggregation
Ocean fertilisation

ABSTRACT

The May 2008 eruption of Chaitén volcano, Chile, provided a rare opportunity to measure the long-range transport of volcanic emissions and characteristics of a widely-dispersed terrestrial ash deposit. Airborne ash mass, quantified using thermal infrared satellite remote sensing, ranged between 0.2 and 0.4 Tg during the period 3–7 May 2008. A high level of spatiotemporal correspondence was observed between cloud trajectories and changes in surface reflectivity, which was inferred to indicate ash deposition. The evolution of the deposit was mapped for the first time using satellite-based observations of surface reflectivity.

The distal (>80 km) ash deposit was poorly sorted and fine grained, and mean particle size varied very little beyond a distance >300 km. There were three particle size subpopulations in fallout at distances >300 km which mirror those identified in fallout from the 18 May 1980 eruption of Mount St. Helens, known to have a high propensity for aggregation. Discrete temporal sampling and characterisation of fallout demonstrated contributions from specific eruptive phases. Samples collected at the time of deposition were compared to bulk samples collected months after deposition and provided some evidence for winnowing.

Experimentally-derived ash leachates had near-neutral pH values and charge balance which indicates minimal quantities of adsorbed acids. X-ray Photoelectron Spectroscopy (XPS) analyses revealed surface enrichments in Ca, Na and Fe and the presence of coatings of mixed Ca-, Na- and Fe-rich salts on ash particles prior to deposition. Low S:Cl ratios in leachates indicate that the eruption had a low S content, and high Cl:F ratios imply gas–ash interaction within a Cl-rich environment. We estimate that ash fallout had potential to scavenge ~42% of total S released into the atmosphere prior to deposition. XPS analyses also revealed ash particle surfaces were strongly enriched in Fe (in contrast to the results from bulk leachate analyses), which suggests that Chaitén ash fallout over oceans had potential to influence productivity in high-nutrient, low-chlorophyl regions of the oceans. Therefore ash particle surface geochemical analysis should be applied to quantify Fe-modulated biologically-forced CO_2 draw-down potential of volcanic ash fallout over oceans.

1. Introduction

Ash fallout from explosive volcanic eruptions is rarely deposited in entirety on terrestrial surfaces and some fraction inevitably ends up deposited in the oceans. The May 2008 eruption of Chaitén volcano, Chile, provided a rare opportunity to measure the dispersion and long-range transport of volcanic emissions in the lower stratosphere, and characterise associated fallout over a largely terrestrial setting. Clouds from the eruption deposited ash over Chile and Argentina and formed the first continental-scale ash deposit since the eruptions of Mount St. Helens in 1980 and Cerro Hudson in 1991. Adsorbed soluble (ephemeral and mobile) chemical components related to eruption of volcanic gases and associated incrustations may generate a range of direct and indirect biological, chemical and physical effects following deposition into terrestrial and aquatic ecosystems (Óskarsson, 1980; Witham et al., 2005).

* Corresponding author at: Climate and Atmosphere Department, Norsk Institutt for Luftforskning, Instituttveien 18, P.O. Box 100, NO-2027 Kjeller, Norway.
E-mail address: adu@nilu.no (A.J. Durant).

1474-7065/$ - see front matter © 2011 Elsevier Ltd. All rights reserved.
doi:10.1016/j.pce.2011.09.004

The type and magnitude of these impacts depend on various factors, including the ash chemical and physical properties, deposit thickness and residence time, and sensitivity of the local environment. Although a large number of eruptions have been investigated (Witham et al., 2005), this is the first such investigation of a rhyolitic ash-fall and the environmental effects of associated rhyolitic ash leachates.

In this study, we analyse: (1) changes in airborne ash mass in the volcanic clouds produced by the eruption as a function of time from satellite observations and related to observed fallout; (2) sedimentological characteristics of ash fallout collected at or very near the time of deposition, i.e., pristine and unaffected by hydrological or aeolian processes post-deposition; and (3) the composition of chemical leachates released through deposition of rhyolitic ash fallout in aqueous environments.

1.1. The May 2008 eruption of Chaitén, Chile

The eruption chronology reported here combines previous accounts (Carn et al., 2009; Folch et al., 2008; Lara, 2009; Watt et al., 2009) and additional surface and remote sensing observations of the eruption (Table 1). The May 2008 eruption of Chaitén was unexpected as the previous documented eruption at the volcano occurred nearly 10,000 years ago (Naranjo and Stern, 2004) though new tephrochronological data from surface and lake records in Argentina suggest that there were other important explosive events during the Holocene (Iglesias et al., 2011). Seismic activity increased on 30 April 2008 with swarms of volcano-tectonic earthquakes ranging in magnitude from 3 to 5 (Carn et al., 2009). Between 1 May and 2 May 2008 the frequency of events increased and reached a maximum of 15–20 per hour prior to the first major eruption (Phase 1) at ~08:00 UTC on 2 May (Table 1) that generated a column in excess of 21 km above mean sea level (MSL) (Lara, 2009). Geostationary Operational Environmental Satellite (GOES) thermal infrared imagery indicated a cloud height of 12 km MSL at 0800 UT on 2 May 2008 (Carn et al., 2009) for the dispersed part of the cloud which was corroborated a day later by cloud height estimates from a space-borne lidar (CALIOP; Thomason and Pitts, 2008). After a period of quiescence on the morning of 3 May 2008, Phase 2 of the eruption was initiated by a large column that reached 17–20 km MSL (observed by G. Villarosa at 14:15 ART/17:15 UTC) from the surface at a location near Esquel, Argentina (42.9°S 71.317°W), 124 km from the volcano). Low level ash emission continued to sustain an ash column with height of <10 km MSL between 3 and 5 May (Watt et al., 2009). Phase 3 of the eruption initiated on 6 May 2008 and generated a column that was estimated to have reached in excess of 30 km (GOES observations at 1200 UT on 6 May 2008) (Carn et al., 2009). Airborne ash and/or ice-coated ash in the dispersed cloud from this phase was observed using CALIOP at a height of ~16 km MSL the following day between 41 and 42°S (Thomason and Pitts, 2008). Phase 4 began on 8 May 2008 with the eruption of an ash column to 20–22 km MSL. Volcanic aerosol from this phase was observed using CALIOP at a height of 13 km MSL the following day (Carn et al., 2009; Thomason and Pitts, 2008). Emission continued into May and June at low intensities with ash columns generally reaching mid- to upper tropospheric heights. By July activity had diminished and occasional ash eruptions generated plumes that reached between <2 and 3 km (Simkin and Siebert, 2002).

Ash fallout from the eruption was widespread and impacted large regions of Chile and Argentina (Watt et al., 2009). Ash emissions from Phase 1 were dispersed to the southeast over Argentina, although an early emissive pulse on 2 May was transported to the east and northeast of Chaitén volcano, and ash fallout was observed at Esquel, Argentina (42.907°S 71.308°W), ~110 km away from Chaitén volcano and Epuyén (42.233°S 71.350°W) ~130 km to the northeast (Fig. 5). Ash fallout was observed at Comodoro Rivadavia on the Argentine coast (45.87°S 67.48°W) over 500 km to the SE approximately 16 h after the eruption began. A sheared portion of the cloud was transported to the NW as far as Bariloche, Argentina (41.16°S 71.34°W), about 215 km NNE of Chaitén in the evening of 2 May 2008, although no ash-fall was reported at the time.

Emissions from Phases 2–4 were dispersed first to the southeast towards Comodoro Rivadavia on 3 May, and then east towards the Argentine coastal settlements of Trelew (43.249°S 65.307°W) and Puerto Madryn (42.754°S 65.049°W) where ash fallout was observed on 5 May. Ash emissions from Phase 3 of the eruption (Table 1) were carried to the northeast on 6 May and reached Neuquén,

Table 1
Eruption chronology for the May 2008 eruption of Chaitén volcano, Chile.

Phase	Date	Time (UTC)	Observation	Cloud height (location)	Measurement source	Reference
1	2 May 2008	08:00–14:00	Initial explosive ash column	>21 km (Chaitén volcano)	Visual observation (PIREP)	(Carn et al., 2009; Folch et al., 2008)
		Morning	Early column activity	10.7–16.8 km	Visual observation (SGVP)	(Folch et al., 2008)
			Stratospheric cloud height	12 km	GOES imagery	(Carn et al., 2009)
2	3 May 2008	18:15	Explosive ash column	17.4–19.6 km	Visual observation (clinometer)	G. Villarosa
	3–5 May 2008		Sustained explosive ash emission	<10 km (Chaitén volcano)		(Watt et al., 2009)
	3–4 May 2008		Fine volcanic ash and/or ice crystals	~12 km (30°S)	CALIOP/OMI	(Carn et al., 2009)
3	6 May 2008	12:00*	Initial explosive ash column	30 km (Chaitén volcano)		(Carn et al., 2009)
	6 May 2008	13:30*	Initial explosive ash column	30 km (Chaitén volcano)	Visual observation (ONEMI)	(Folch et al., 2008)
		20:00	Increase in eruption intensity			(Folch et al., 2008)
	7 May 2008		Eruption column	7–10 km	CALIOP	(Folch et al., 2008)
	7 May 2010		Ash / ice-coated ash cloud	~16 km (41–42°S)		(Thomason and Pitts, 2008)
4	8 May 2008	03:30	Initial explosive ash eruption	20–22 km (Chaitén volcano)	GOES imagery	(Carn et al., 2009)
	8 May 2008		Airborne ash	3–10 km (Buenos Aires)		(Folch et al., 2008)
	9 May 2008		Volcanic aerosol	13 km	CALIOP	(Carn et al., 2009)

CALIOP – Cloud-Aerosol Lidar with Orthogonal Polarisation (on Cloud-Aerosol Lidar and Infrared Pathfinder Satellite Observations platform).
GOES – Geostationary Operational Environmental Satellite.
OMI – Ozone Monitoring Instrument.
ONEMI – Oficina Nacional de Emergencia del Ministerio del Interior (National Office of Emergency of the Interior Ministry, Chile).
PIREP – Pilot report.
SGVP – Smithsonian Global Volcanism Program.
* These reports conflict on the time of onset of the initial activity of Phase 3.

Argentina (38.949°S 68.066°W), approximately 575 km northeast of Chaitén, some 8–14 h after the initial eruption. On 7 May, the first ash fall was observed at Bariloche and later ash fallout was observed at Bahía Blanca (38.711°S 62.268°W) and Mar Del Plata (37.980°S 57.590°W), approximately 1000 km and 1400 km, respectively, from Chaitén. Ash emissions from Phase 4 (Table 1) were carried to the north via Neuquén, and then to the northwest as far as Concepcion, Chile (36.81°S 73.03°W) over 650 km to the north northwest by 1600 UTC on 8 May 2008. Ash fallout after this time was minimal other than a later explosive pulse on February 19 2010 that produced a deposit that extended over 200 km southeast from Chaitén volcano.

There were three stratigraphic units (α, A-M, β) identified in deposits within 25 km of the volcano formed from activity between the periods 1–2, 3–5, and 6 May, respectively (Alfano et al., 2010). Unit α was mapped to the northeast, A–M to the southeast and β again to the northeast. The distal (~>100 km) deposit from the May 2008 eruption comprised $\sim 1 \times 10^{11}$ kg ash (dense rock equivalent, DRE ~0.07 km^3) which was deposited over 2×10^5 km^2 (Watt et al., 2009). The erupted tephra consisted of ash (~80 wt.%), pumice lapilli and bombs (17 wt.%), and obsidian fragments (~3 wt.%). Compositional analysis of pumice indicated that a crystal-poor rhyolitic (73–76 wt.% silica content) magma with ~1.3–2.3 wt.% water (H_2O and OH^-) was erupted during the May 2008 event (Alfano et al., 2010; Castro and Dingwell, 2009). Satellite observations (Ozone Monitoring Instrument) indicated the collective mass of SO_2 released from all phases of the eruption only totalled ~10 kT (Carn et al., 2009). The quantity of respirable (<4 μm) particles in ash fallout from the eruption ranged from 8.8 to 11.9 vol.% and contained 2.2–7.4 wt.% cristabolite, which posed a low human health hazard (C. Horwell, personal communication 2011). Approximately 400 km^2 of native evergreen forest were damaged by the 2008 eruption of Chaitén (Pallister et al., 2010) and in areas beyond the blast-affected zone, tephra fallout stripped foliage and branches from the forest canopy. There were numerous impacts on agriculture and infrastructure (Wilson et al., 2009a,b).

2. Methods

2.1. Satellite data analysis

MODIS infrared and visible radiances were analysed to assess the amount of fine ash suspended in the atmosphere and to estimate the area of land covered by ash fallout from the Chaitén eruption. The infrared data were used to retrieve particle effective radii (r_{eff}, weighted mean of the ash particle size distribution), infrared optical depth and mass loadings (g m^{-2}) using a combined radiative transfer and ash microphysical model (Prata and Grant, 2001; Wen and Rose, 1994). The ash microphysical component assumes airborne ash is composed of spherical particles with a modified gamma particle size distribution and a rhyolitic composition. The wavelength dependent refractive indices were taken from Pollack et al. (1973); this composition improves results over assumed andesitic or basaltic refractive indices (Gangale et al., 2010). The total mass of fine ash in each MODIS image was calculated by finding the sum of each pixel mass loading (nominally 1 km^2) multiplied by the area of the cloud. The methodology may generate underestimations mostly due to the presence of highly opaque clouds, and overestimations due to uncertainty in the underlying assumptions, highly transparent clouds and noisy data. This leads to a typical error in cloud mass estimates of around 20%.

The infrared-derived mass loadings were complemented by analyses of visible light reflected from the surface, also using MODIS data, to estimate the surface area impacted by ash fallout as a function of time. The assumption underlying the analysis is simple: ash fallout modifies surface albedo and MODIS measures the directional surface reflectance at several wavelengths. We used a combination of MODIS channels, and through trial-and-error found a subset that was best able to indentify changes in reflectances associated with ash fallout. The directional reflectances were normalised by geometrical factors that depend on the solar and satellite viewing angles. No attempt was made to relate the changes in reflectance to the accumulation of ash on the ground, instead each image was analysed to estimate the area difference in area from a reference image, taken as containing the least clouds over the preceding 2 weeks prior to the eruption. Difficulties were found in estimating these changes in regions of rapid topographic change (e.g. the eastern side of the southern Andes) and these areas were masked out.

2.2. Deposit characterisation

An ash collection network was set up in Argentina in cooperation with national, provincial and municipal agencies. Fallout over the Andean region was collected using traps and sampled specific ash fall events related to discrete phases of the eruption (or shortly after every ash fall event) over a vast area within 250 km of the volcano (Figs. 5 and 6; Table 2). In some cases samples were collected within hours and up to 5 days after deposition by non-specialists (including engineers and park rangers). These samples may have been exposed to light precipitation and different degrees of winnowing (Table 2).

2.3. Particle size analysis

Particle size was measured through application of low angle laser diffraction particle size analysis (Blott et al., 2004) using a Malvern Instruments Mastersizer 2000. In this technique, the ash sample is suspended in water, circulated through a measurement cell, and light at different wavelengths (red and blue) is passed through the dispersed sample and the diffraction pattern is measured. Particle size is determined through application of a particle scattering model (Lorenz-Mie) and assumptions are made regarding particle refractive index and shape (spherical particle assumption). In this study we assumed ash samples had a rhyolitic composition and used a refractive index of 1.5 (Horwell, 2007). The instrument returns distributions of volume-based frequency between size classes spanning 0.02–2000 μm.

Particle size subpopulations were identified following the method outlined in Wohletz et al. (1989). The measured particle size distribution of a sample taken from a discrete location may be deconvolved into a series of subpopulations that initially result from fragmentation at the vent (primary magma rupture and secondary fragmentation in the conduit), and are subsequently modified by cloud processing during transport. Microphysical processes (e.g., hydrometeor formation) and gravitational settling result in size selective sorting during transport and sedimentation. Identification of particle size subpopulations may be mapped out to understand the propensity of various processes that modify the initial particle size distribution.

2.4. Leachate analysis

In order to assess the release of chemical species following deposition of the ash material in aqueous environments, extractions were carried out on samples through immersion and agitation in deionized water (ash-to-water ratio of 1:25) for 45 min in an acid-washed polyethylene tube. The slurry was centrifuged and the pH of the supernatant leachate was measured prior to filtration through 0.2 μm cellulose acetate membrane filters. The

Table 2
Summary of samples collected in this study.

Sample ID	Collection date	Collection time	Eruption date	Latitude	Longitude	Distance (km)	Comments
CH0805_1	4 May 2008		2–4 May 2008	−43.176531°	−71.550786°	97.4	
CH0805_2	9 May 2008		2–4 May 2008	−43.123936°	−71.552567°	95.4	
CH0805_3	6 May 2008		2–4 May 2008	−43.069028°	−70.940778°	142.2	
CH0805_4	2 May 2008		2 May 2008	−42.911356°	−71.322956°	109.1	No rain
CH0805_5	4 May 2008		3–4 May 2008	−42.911356°	−71.322956°	109.1	No rain
CH0805_6	6 May 2008		5–6 May 2008	−42.911356°	−71.322956°	109.1	No rain
CH0805_7	9 May 2008		7 May 2008	−42.911356°	−71.322956°	109.1	Direct fallout sampled
CH0805_8	8 May 2008		2–7 May 2008	−42.025883°	−70.804133°	177.4	
CH0805_9	9 May 2008		3–4 May 2008	−43.492419°	−70.810494°	166.7	
CH0805_10	7 May 2008		7 May 2008	−42.081200°	−71.548117°	124.7	Direct fallout sampled
CH0805_11	7 May 2008		3–4 May 2008	−43.250000°	−71.333333°	116.9	
CH0805_12	7 May 2008		3–4 May 2008?	−43.134267°	−71.434117°	104.6	
CH0805_13	7 May 2008		2–7 May 2008	−43.088569°	−71.505208°	97.6	Direct fallout sampled
CH0805_14	7–8 May 2008	20:00–09:00	7 May 2008	−41.124472°	−71.384333°	218.6	Direct fallout sampled
CH0805_15	7 May 2008		3–7 May 2008?	−43.134417°	−71.611444°	91.2	
CH0805_16	7 May 2008		3–7 May 2008?	−43.136300°	−71.438833°	104.5	
CH0805_17	6 May 2008		3–4 May 2008	−43.785694°	−70.934194°	174.8	
CH0805_18	6 May 2008		3–4 May 2008	-44.059361°	−70.394417°	227.9	
CH0805_19	6 May 2008	11:30–13:30	6 May 2008	−42.209683°	−71.405239°	124.3	Direct fallout
CH0805_20	5 May 2008	00:00–9:00	5 May 2008	−42.911356°	−71.322956°	109.1	Direct fallout sampled at Esquel
CH0805_21	4 May 2008	15:05	3–4 May 2008	−43.196167°	−71.607617°	94.2	Some light rain
CH0805_22	4 May 2008	15:24	3–4 May 2008	−43.175450°	−71.691050°	86.9	Some light rain
CH0805_23	4 May 2008	16:18	3–4 May 2008	−43.173600°	−71.749617°	82.6	Some light rain
CH0805_24	3 May 2008	13:40	2–3 May 2008	−42.626350°	−71.065850°	132.1	No rain
CH0805_25	3 May 2008	18:14	3 May 2008	−43.136300°	−71.438833°	104.9	No rain
CH0805_26	6 May 2008		6 May 2009	−41.940000°	−71.493611°	138.6	No rain
CH0805_27	7 May 2008		7 May 2009	−41.940000°	−71.493611°	138.6	No rain
CH0805_28	11 May 2008		3–4 May 2008	−43.185922°	−71.657008°	90.0	
CH0805_29	8 May 2008		6–7 May 2008	−42.178283°	−71.147133°	144.3	
CH0805_30	13 May 2008		3–4 May 2008	−43.541622°	−71.468675°	124.1	
CH0805_31			3 May 2008	−45.867920°	−67.500000°	530.0	
CH0805_32	6 May 2008		2 May 2008	−41.558611°	−69.876944°	182.0	
CH0805_33	8 May 2008		2 May 2008	−43.076944°	−71.462778°	239.6	
CH0805_34	8 May 2008		2 May 2008	−43.139167°	−71.567500°	313.2	

filtered leachates were analysed for SO_4^{2-}, Cl^-, and F^- by ion chromatography (IC), and for Si, Al, Fe, Mg, Ca, Na and K by Inductively Coupled Optical Emission Spectrometry (ICP-OES). Trace element abundances of Cr, Co, Ni, Cu, Zn, As, Se, Sr, Ag, Cd and Pb were determined by Inductively Coupled Mass Spectrometry (ICP-MS), using a three point calibration with standard solutions. Instrumental drift in ICP-OES and ICP-MS results was corrected through periodic measurement against reference sample solutions. X-ray Photoelectron Spectroscopy (XPS) was used to measure the elemental chemistry (composition and speciation) of the uppermost 2–10 nm thick surface layer on selected ash samples (CH0805_33 and CH0805_34). The XPS analyses were carried out at the Leeds EPSCR Nanoscience and Nanotechnology Facility, using a VG Escalab 250 instrument with an Al Kα (1486.6 eV) X-ray source.

3. Results

3.1. Satellite observations of the Chaiten clouds

Fig. 1 shows an interrupted time series of fine ash mass for nine MODIS images analysed for 3–7 May. The total mass of airborne ash ranged from about 0.2–0.4 Tg, which decreased with time, presumably due to losses from ash fallout and dispersion. The spatial distribution of ash mass loading for consecutive MODIS imagery indicates that the eruption cloud was first dispersed to the southeast on 3 May, and then to the east from 5 May (Fig. 2). The area of change (which we attribute to ash fallout) is shown for a series of images starting on 2 May 2010 and ending on 12 May 2010 (Fig. 3). The scale is relative, indicating the number of pixels with a different reflectance signature to that of the reference image. The pixel count is cumulative, but we make no attempt to relate this in a quantitative manner to the build-up of ash on the surface. In

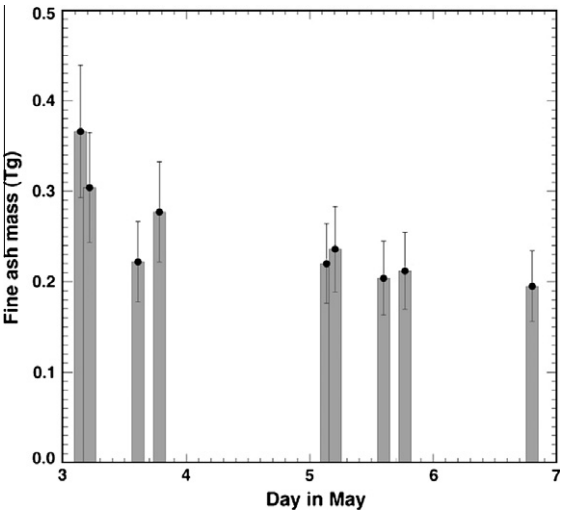

Fig. 1. Mass of fine ash in the atmosphere as a function of time for nine MODIS images. The time series is interrupted because of lack of satellite data coverage and by the sampling rate (up to four times per day).

Fig. 3 we show two images per day (on some days there are as many as four images per day), and there is a high degree of consistency between images obtained on the same day, except at the start of the eruption on 2 May 2010. The pattern of ash fallout broadly follows ash cloud trajectories, although most of the ash is concentrated in a band to the east of the volcano, with a strong branch to the northeast. To illustrate the correspondence between the ash fallout pattern and the fine ash in the atmosphere, the fine

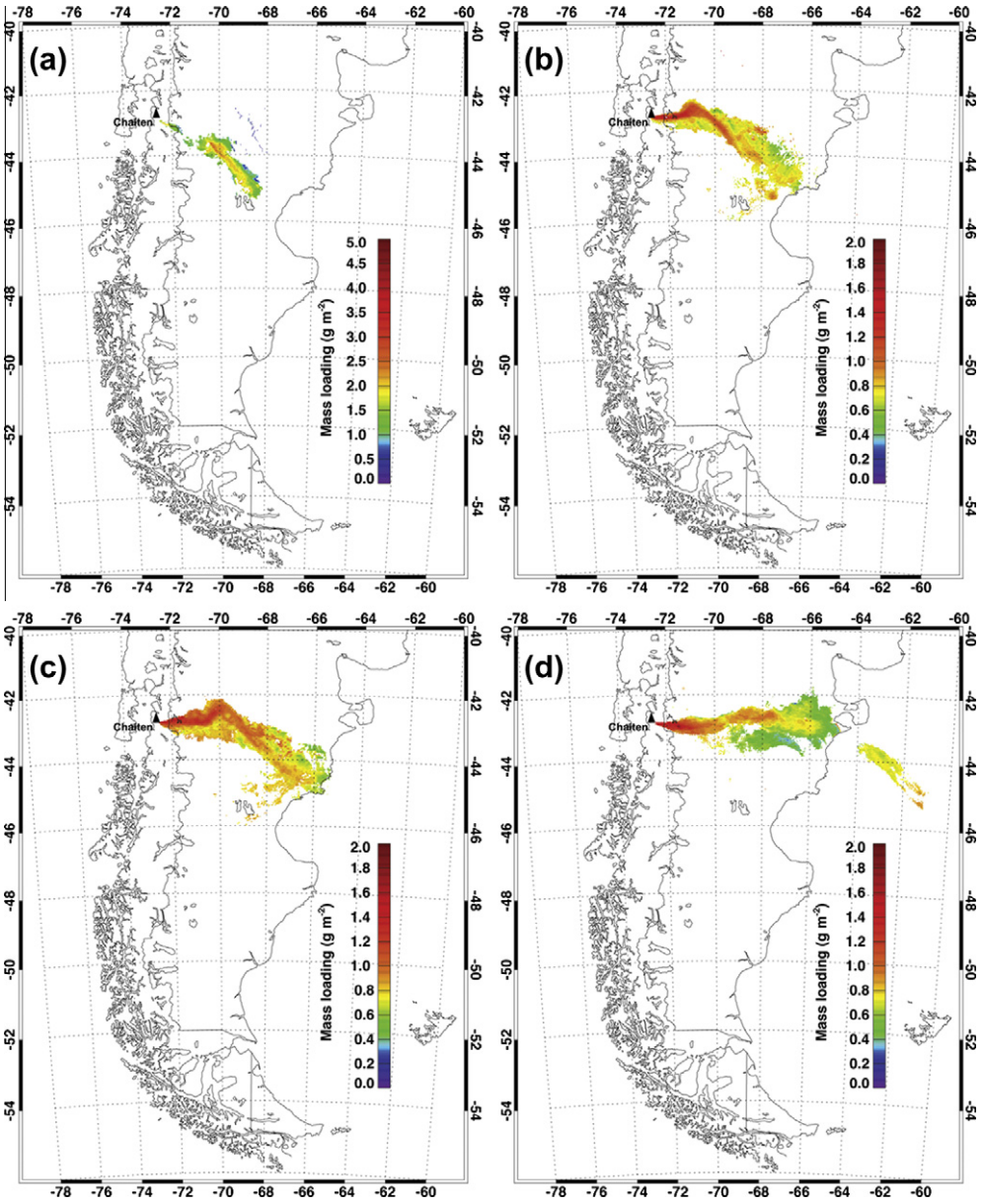

Fig. 2. Fine ash mass loadings retrieved from MODIS infrared satellite measurements for (a) 3 May, 05:19 UTC, (b) 5 May, 03:15 UTC, (c) 5 May, 04:55 UTC and (d) 5 May, 14:20 UTC.

ash mass loading is overlayed onto the areal ash fallout estimate for 5 and 8 May 2010 (Fig. 4).

Volcanic ash retrievals (Fig. 2) clearly show that the ash cloud dispersed to the southeast on 3 May and changed to a more easterly dispersal between 0455 UTC and 1420 UTC on 5 May. This later northwards migration in cloud trajectory is followed by a slight increase in measured surface reflectivity at 1830 UTC on 5 May and 1505 UTC on 6 May (Fig. 3) from ash fallout in the vicinity of Trelew and Rawson near the E coast of Argentina. The dispersal of the deposit from Phase 3 followed a northeast-trending distribution and was first observed in reflectivity measurements at 1915 UTC on 6 May as a lobe developed out towards Maquinchao, Argentina (41.25°S 68.70°W). Reflectivity changes indicate that activity from 7 May up to 12 May continued to build an ENE-trending deposit towards San Antonio and Mar Del Plata on the Argentine coast (40.74°S 64.97°W), that backed round to the NW as far as Concepcion, Chile (Figs. 3 and 4).

3.2. Sedimentological characteristics of the fall deposit

Scanning electron micrographic images (Figs. 7 and 8) indicate Chaitén ash fallout consisted almost entirely of non-vesicular rhyolitic glass, characterised by angular shard-like morphologies, and a subordinate component of blocky pyroclasts; all particles had a sugary appearance due to coatings of very small particles. Overall ash fallout from the Chaitén eruption was poorly sorted and consisted of particles that varied in diameter by more than two orders of magnitude (1 to >100 μm or about 3.25 to 10∅); even at close proximity to the volcano the deposit was remarkably fine grained and did not vary markedly with distance (Fig. 9). For the 2–5 May 2008 phase, the mean particle size of the deposit remained fairly consistent at 32 μm ± 5 μm between 95 and 530 km distance from the volcano. In contrast, for the 6–7 May 2008 phase, the deposit was coarser and mean particle size was 90 μm ± 109 μm between 98 and 144 km from the volcano.

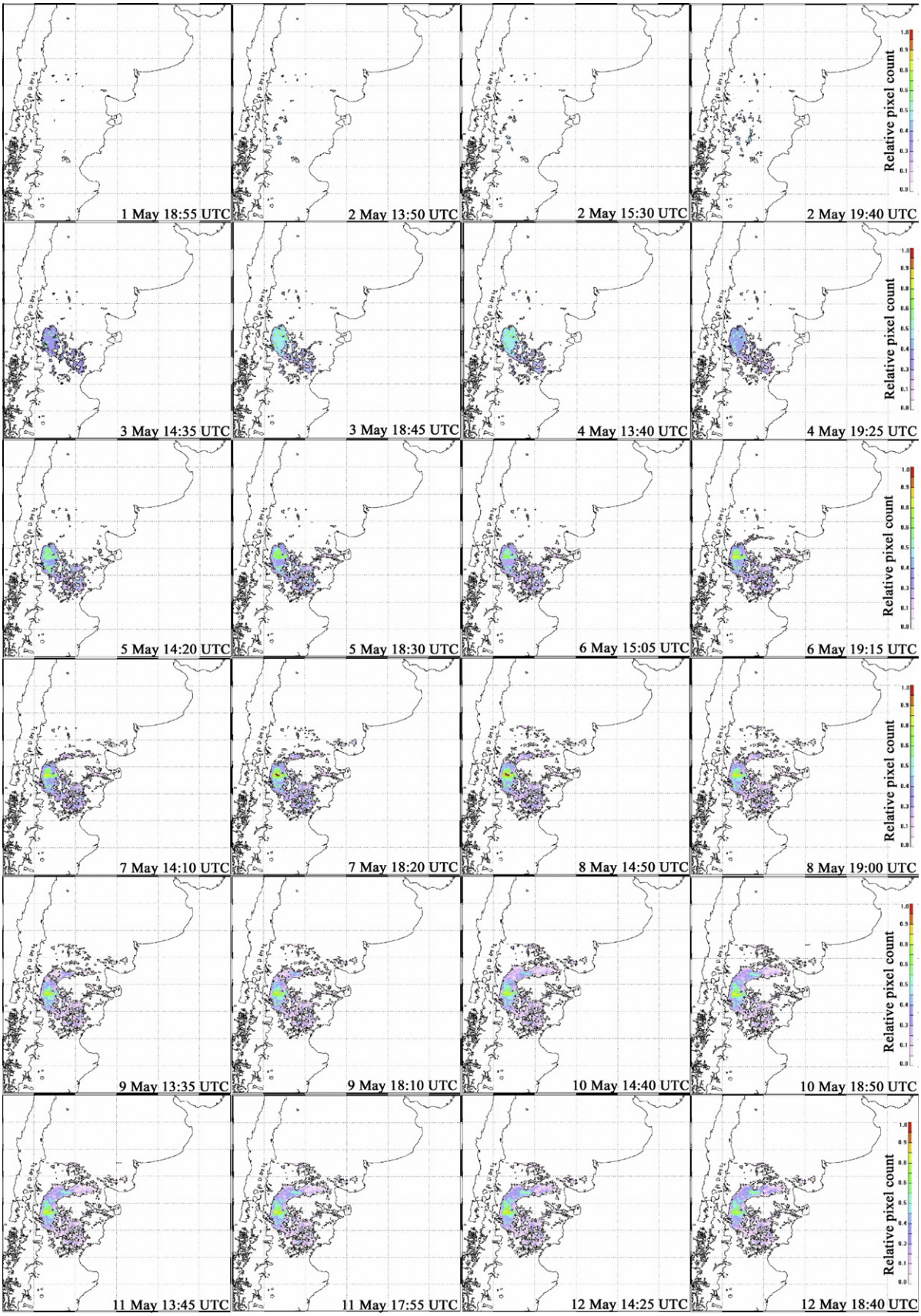

Fig. 3. Areal estimates of ash fallout on the ground based on MODIS visible reflectances. Each panel shows analyses from a single MODIS image (two per day are shown), with the colours representing the cumulative count of pixels deemed to have changed above a threshold based on a reference image obtained prior to the eruption. The scale is a relative measure with red representing more pixels affected and purple less pixels affected. (For interpretation of the references to colour in this figure legend, the reader is referred to the web version of this article.)

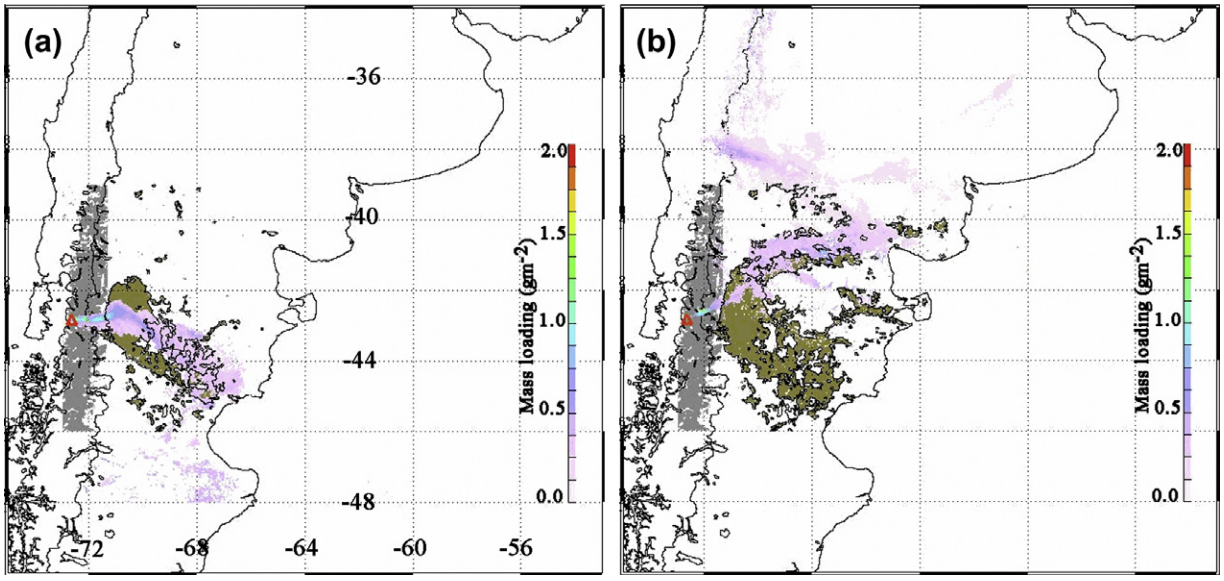

Fig. 4. Fine ash in the atmosphere (colour scale on right side) and an estimate of ash fallout based on MODIS visible reflectance (mauve) for (a) 5 May and (b) 8 May. The grey-coloured region is an area where the algorithm to estimate reflectance change failed due to the nature of the land surface (large topographic variability).

Fig. 5. Top left: thin ash deposit from the May 2 ash fall at El Hoyo (42.075°S 71.510°W), 12 km south from El Bolsón, Argentina, on the morning of May 3; top right: concurrent rainfall and ash fallout on 4 May 2008 (photograph Valeria Outes); bottom left: ash layer at Futaleufú border control post in Argentina (sample CH805_23) on 4 May – note the nature of the contact with white ash directly overlying soil (photograph G. Villarosa); bottom right: View of the ash deposit in Tecka, 75 km SE from Esquel, on May 4 (photograph G. Costa).

Particle size subpopulations were identified in fallout from the eruptions (Fig. 10): there were a total of five subpopulations at distances <250 km from the volcano and only three subpopulations were present in fallout >500 km in fairly consistent mass proportions. The main distance changes to note were the disappearance of coarse mode ash, while prominent smaller modes persisted at greater distance in fairly consistent mass fractions.

3.3. Soluble element chemistry

The pH and major and trace element concentrations in the ash leachates are given in Tables 3 and 4. The charge balance was less than ~15% in all but two samples (CH0805_24 and CH0805_30), and the pH values were consistently close to neutral. The major elements in the fresh ash leachates were Cl (1.5–9.7 mmol/kg),

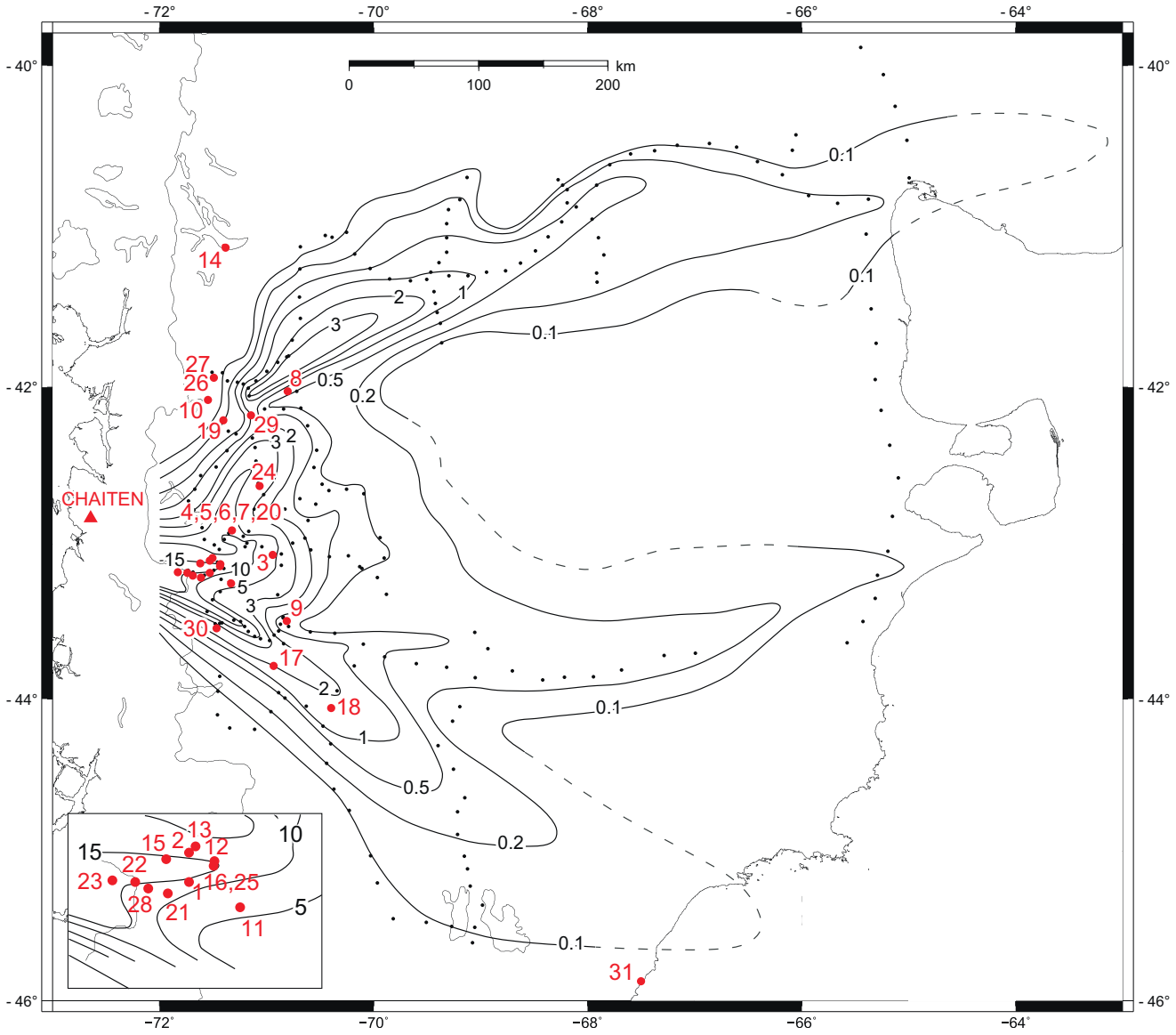

Fig. 6. Isopach map of fallout from the 2008 Chaitén eruption courtesy of S. Watt. The isopach contours are in mm from Watt et al. (2009); the small black dots are measurement locations in the Watt et al. study. Sample locations reported in this study are shown in red and are identified by the last two digits of the sample ID detailed in Table 2. The map inset shows detail of the sample cluster ~100 km from the volcano. (For interpretation of the references to colour in this figure legend, the reader is referred to the web version of this article.)

followed by Na (0.9–4.1 mmol/kg), Ca (0.6–4.4 mmol/kg) and S (0.1–2.9 mmol/kg). Fluoride occurred at concentrations ranging from 0.2 to 1.5 mmol/kg. The most abundant trace elements were Zn, Cu and As (~0.2–15 μmol/kg), while Cr, Co, Ni, Se, Sr, Ag, Cd and Pb were found in significantly lower concentrations. Dissolved Fe amounted to $\sim 10^{-4}$–2.7×10^{-2} μmol/kg. Leachate compositions of the fresh ash samples were not distinguishable from those of the ash specimens which had been exposed to light rain or for which no information was available (Tables 3 and 4). The total dissolved solid concentration in the ash leachates averaged to 13.5 ± 4.4 mmol/kg. Further, we did not observe a trend in the ash leachate chemistry with distance from the source, and the most distal ash sample (CH0805_31) produced a leachate composition comparable to samples collected closer to the volcano. In addition to the major rock-forming elements, Cl and F (but not S) were detected by XPS in the surface of CH0805_33 and CH0805_34 ash materials.

4. Discussion

4.1. Particle emissions from Chaitén in the context of the global atmospheric silicate particulate cycle

The global annual ash particle flux to the atmosphere is poorly quantified and previous estimates are generally based on historic eruption records and proxies for volcanic ash emission. The proportion of fine ash generated during explosive volcanic eruptions varies according to eruptive style (Mastin et al., 2009; Rose and Durant, 2009), and is primarily a function of magma viscosity, volatile content and open porosity (e.g., Kueppers et al., 2006). Interaction with external water increases the proportion of fine particles (Mastin, 2007; Wohletz, 1983), in addition to comminution and elutriation in pyroclastic flows (Dartevelle et al., 2002; Horwell et al., 2001), and brittle–ductile fracturing during extrusion of magma bodies (Tuffen et al., 2008). The blocky pyroclasts

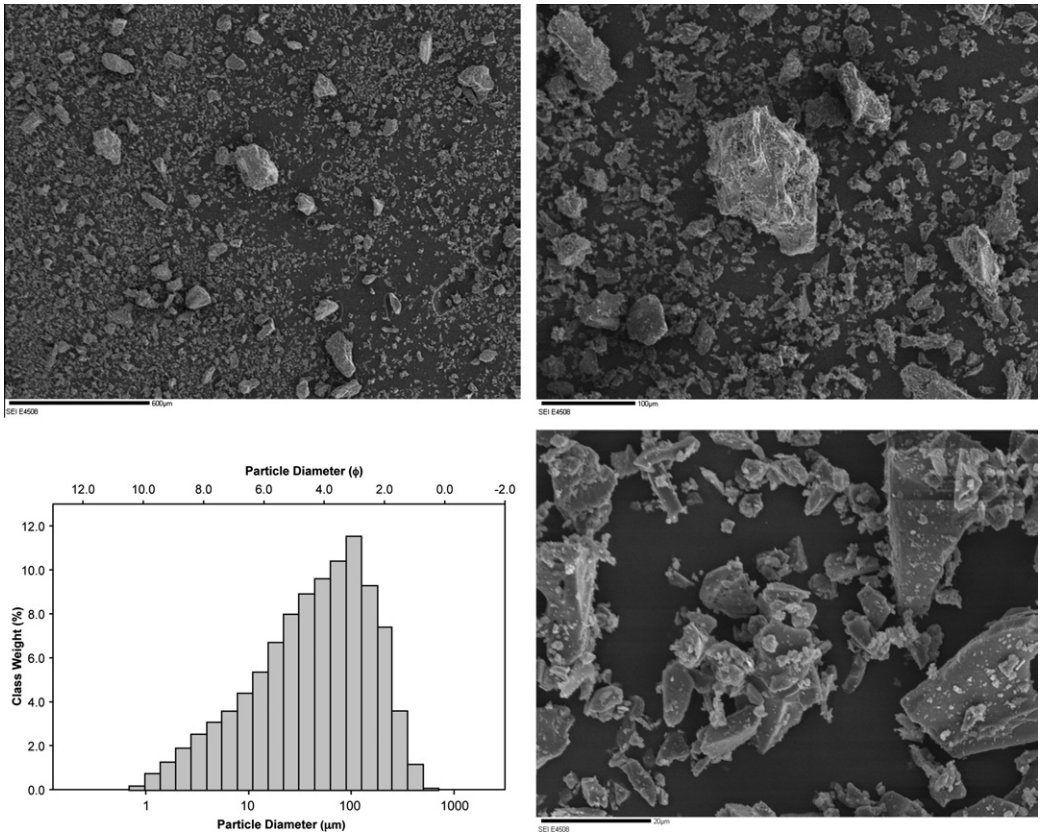

Fig. 7. SEM images demonstrating the poor sorting of ash fallout at Esquel, 109 km E of Chaitén on 2 May 2008. Note larger mode at 300 μm diameter pyroclasts and fine mode at 20–40 μm. All pyroclasts have sharp angular edges and very fine particles adhere to larger ones.

observed in SEM imagery were probably formed during interaction of the magma with external water: the 2008 eruption took place in a small caldera that contained at least two small water bodies next to the dome, and the volcano is located in a region of intense precipitation (>3000 mm/year).

Volcanic ash emissions are episodic events that contribute approximately an order of magnitude less silicate particles to the atmosphere on average than that contributed by the mineral dust cycle (Cakmur et al., 2006). To place this in global context, the total mass of global emissions of fine ash may be estimated from historic records of eruption frequency (e.g., Deligne et al., 2010; Pyle, 2000) and assumptions on the proportion of fine ash generated by different styles of explosive volcanism. Recent observations indicate the total fraction of fine ash (diameter < 63 μm, m_{63}) emitted during explosive volcanic activity varies between 2 wt% for small basaltic eruptions to 60 wt% for explosive silicic eruptions (Mastin et al., 2009). The annual total mass of fine ash (particles < 63 μm) emitted to the atmosphere is estimated at approximately 176–256 Tg based on 1000 year average eruption frequencies and an assumed m_{63} proportion of 20 wt.% (Durant et al., 2010). Of this total, the vast majority of ash emitted is from magnitude 6.5 eruptions which emit up to 3.2×10^{13} kg of total erupted mass. The 2008 Chaitén eruption emitted between 5 and 10×10^{11} kg of tephra between May 2008 to Jan 2009 (Alfano et al., 2010) which corresponds to a magnitude 4.5–5.0 on the scale of Pyle (2000); eruptions of this scale account for between 15% and 22% of the global 1000 year average annual budget (Durant et al., 2010). Assuming 20–50 wt% total mass erupted was finer than 63 microns, this eruption contributed between 40 and 290 wt% of the total global average annual fine ash (m_{63}) emission for 2008.

4.2. Correlation of ash emission and observed fallout

At any moment during the period 3–7 May 2008 there was between 0.2 and 0.4 Tg of airborne ash <30 μm diameter suspended in the atmosphere (Fig. 1). MODIS retrievals indicated the cloud contained an abundance of fine ash with particle effective radii spanning 1 μm < r_{eff} < 16 μm. This range is somewhat smaller than found in earlier studies of volcanic ash clouds (e.g., Prata and Grant, 2001; Wen and Rose, 1994), with typical sizes of 3–5 μm, compared to 3–8 μm found previously. The spatial distribution of ash mass loading for consecutive MODIS imagery is governed by the winds, source strength and loss processes; imagery between 3 and 5 May showed a prominent change in transport direction from the southeast to the east (Fig. 2). Using satellite-based reflectance measurements, the deposit was mapped out chronologically as it formed and closely follows the trajectory of eruption clouds (Fig. 4). The approach reported here is the first time that such a methodology has been applied to observe the formation of a bulk ash deposit evolving from discrete eruptive events over time. Consequently, it is possible to relate the bulk sedimentological characteristics of the deposit measured at a discrete location to observed fallout from specific eruptive events.

A number of the samples were collected in succession at the same location and capture fallout from more than one eruptive phase (Table 2). For example, there were at least two fall units identified at Bolson, Argentina (CH0805_26, CH0805_27, and CH0805_8, collected on 6, 7, and 8 May, respectively). These are compared to bulk samples collected later in the same vicinity by Watt et al. (2009) which appear to have composite features of the individual fallout events (Fig. 11). There were also at least four discrete fall units identified through systematic sequential

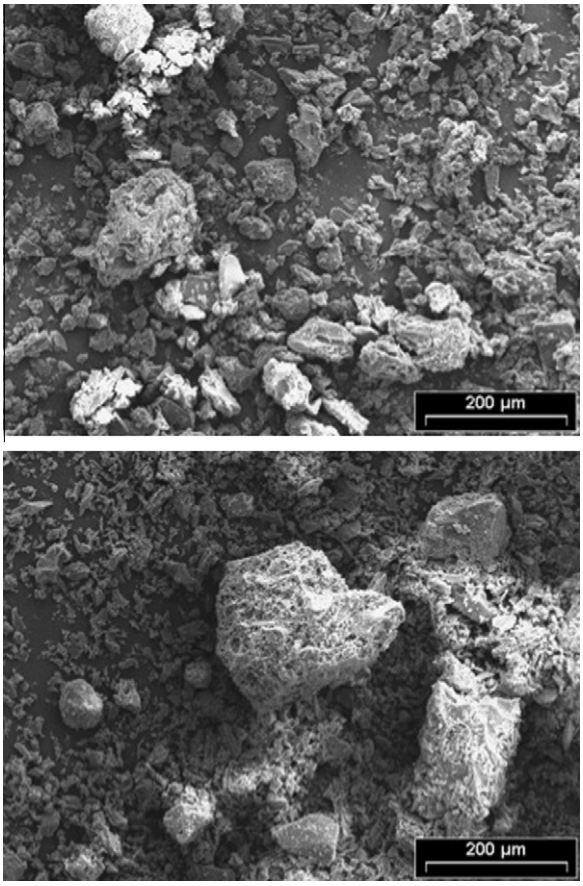

Fig. 8. SEM images of ash aggregates after breaking up on impact at locations CH805_23 (above) and CH805_24 (below) (images courtesy of Valeria Outes at Centro Atómico Bariloche facility).

sampling at Esquel, Argentina (CH0805_4, CH0805_5, CH0805_6 and CH0805_7, collected on 2, 4, 6, and 9 May, respectively). The variation in particle size characteristics between sequential fallout, and between bulk deposits formed by multiple phases, is related to variability in eruption source parameters (such as eruption intensity which affects the initial particle size distribution), sorting

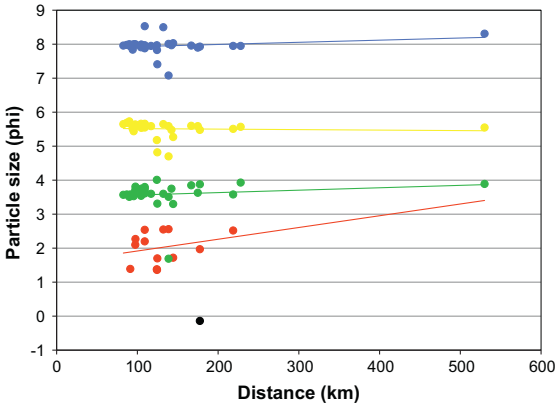

Fig. 10. Particle size subpopulations identified as a function of distance from the volcano. Distal fallout (500 km) consisted of three particle size subpopulations and an additional coarse subpopulation was present in fallout ~80–250 km from the volcano.

during transport (the duration of which is related to emplacement height and the wind field), and particle size selective processes acting during sedimentation (e.g., aggregation). Importantly, this kind of analysis demonstrates how ash deposits may be composed of fallout from many different phases of a given eruption, so care must be taken when using measurements of discrete fallout samples to reconstruct eruptions source parameters, such as initial particle size distribution, and during interpretation of polymodal particle size distributions. Therefore there is a real need for time-resolved sampling of ash fallout in order to accurately reconstruct eruption source parameters.

Ash winnowing has been interpreted by many investigations of distal ash fallout as a process which redistributes ash substantially and modifies sedimentological characteristics over periods as long as months or years after deposition (e.g., Rose et al., 2003; Scasso et al., 1994). The Watt et al. samples were collected weeks after deposition and do show significant but variable particle size differences from our samples which were collected before winnowing (e.g., Fig. 11). These differences will be the focus of a future study dedicated to winnowing and we use only the "unwinnowed" materials to look for particle size differences in this study.

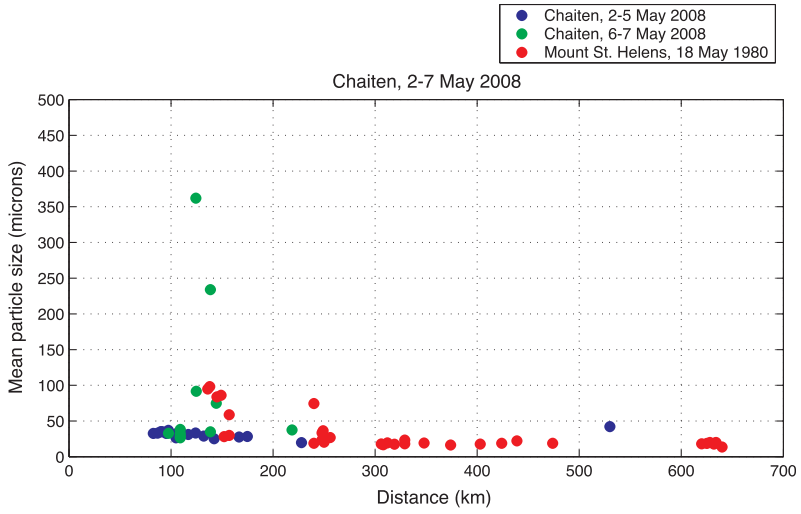

Fig. 9. Particle size as a function of distance from the volcano. The data are separated into Phases 1–2 (2–5 May) and Phases 3–4 (6–7 May). Particle size data from the 18 May 1980 eruption of Mount St. Helens are also shown.

Table 3
Concentrations of major, minor and trace elements removed from the Chaitén ash by deionized water leaching solution.

Sample ID	Si	Al	Mg	Ca	Na	K	F	Cl	SO_4	S/Cl	Cl/F	Cr	Mn	Fe	CO	Ni	Cu	Zn	As	Se	Ag	Cd	Pb
	mmol kg^{-1} ash											μmol kg^{-1} ash											
Phase 1																							
CH0805_01	0.61	0.16	0.59	2.07	3.28	0.35	0.97	7.10	1.44	0.20	7.28	0.004	49.54	15.91	0.024	0.064	0.66	5.455	2.26	0.055	0.161	0.003	<d.l.
CH0805_02	0.46	0.08	0.58	3.33	3.04	0.96	0.66	8.03	1.76	0.22	12.26	<d.l.	40.13	5.69	0.025	0.075	0.26	0.398	14.54	0.086	0.099	0.001	<d.l.
CH0805_04	0.51	0.10	0.48	0.63	3.38	0.28	0.53	7.90	1.00	0.13	14.85	0.009	1.72	0.80	0.010	0.066	0.46	<d.l.	<d.l.	0.067	0.049	<d.l.	<d.l.
CH0805_05	0.35	0.09	0.29	1.06	2.35	0.40	0.95	5.83	0.36	0.06	6.17	0.002	23.50	3.22	0.018	0.037	0.35	5.192	0.21	<d.l.	0.046	0.002	<d.l.
CH0805_09	0.52	0.04	0.76	4.22	3.07	0.36	1.15	5.72	2.73	0.48	4.99	<d.l.	12.66	0.15	0.014	0.076	0.37	<d.l.	<d.l.	0.042	0.032	0.000	<d.l.
CH0805_11	0.45	0.08	1.17	2.75	2.35	0.29	1.50	9.30	0.92	0.10	6.22	0.020	23.25	8.17	0.022	0.052	0.31	0.175	4.09	0.004	0.031	<d.l.	<d.l.
CH0805_17*	0.49	0.13	0.40	0.89	1.81	0.49	0.20	4.79	0.31	0.06	23.71	0.043	29.05	13.36	0.033	0.058	0.54	2.293	1.03	<d.l.	0.018	0.001	<d.l.
CH0805_18*	0.60	0.17	0.29	0.64	1.58	0.73	0.93	3.85	0.54	0.14	4.16	<d.l.	18.14	15.86	0.018	0.038	0.34	5.947	0.44	0.017	0.014	0.002	0.001
CH0805_20	0.22	0.06	0.31	0.96	2.46	0.87	0.88	6.04	0.37	0.06	6.83	<d.l.	22.92	0.10	0.020	0.043	0.35	3.307	0.09	<d.l.	0.014	0.001	<d.l.
CH0805_21	0.38	0.09	0.65	3.03	3.21	0.66	0.96	7.62	1.70	0.22	7.96	0.045	30.97	8.95	0.021	0.121	0.60	1.702	11.38	<d.l.	0.017	0.002	0.002
CH0805_22	0.40	0.09	0.25	1.06	0.94	0.43	0.79	2.88	0.40	0.14	3.63	<d.l.	15.23	7.46	0.011	0.024	0.46	3.636	3.22	<d.l.	0.011	0.000	<d.l.
CH0805_23	0.32	0.07	0.43	1.52	2.61	0.19	0.85	6.15	0.91	0.15	7.28	<d.l.	27.13	4.54	0.014	0.033	0.28	0.779	2.73	0.013	0.013	0.002	<d.l.
CH0805_24	0.82	0.06	0.55	4.40	3.34	0.31	1.17	5.11	2.43	0.48	4.35	0.011	10.11	1.16	0.009	0.080	0.40	0.278	<d.l.	0.045	0.012	0.001	0.000
CH0805_25	0.78	0.02	0.69	4.17	2.85	0.46	1.35	4.55	2.88	0.63	3.38	0.077	6.83		0.015	0.230	0.65	0.139	<d.l.	0.025	0.012	0.001	<d.l.
CH0805_28	0.29	0.07	0.72	2.36	4.11	0.50	1.25	9.71	1.49	0.15	7.74	<d.l.	50.12	3.71	0.027	0.086	0.36	3.115	1.82	0.000	0.011	0.002	<d.l.
CH0805_30	n.a.	0.00	0.42	1.86	3.45	0.56	0.25	1.50	2.09	1.40	5.89	n.a.	n.a.	n.a.	n.a.	n.a.	n.a.	n.a.	n.a.	n.a.	n.a.	n.a.	n.a.
CH0805_33	0.74	0.06	0.24	1.15	3.64	0.05	0.29	5.13	1.69	0.33	17.94	Iq.010	8.34	3.62	0.007	0.033	0.73	I < d.l.	18.11	0.002	0.179	0.002	10.001
CH0805_34	n.a.	0.00	0.21	1.96	2.30	0.07	0.47	6.76	0.97	0.14	14.49	n.a.	n.a.	n.a.	n.a.	n.a.	n.a.	n.a.	n.a.	n.a.	n.a.	n.a.	n.a.
Phase 2																							
CH0805_06	0.26	0.06	0.36	0.87	2.06	0.27	0.21	5.56	0.13	0.02	27.05	0.004	34.46	2.86	0.027	0.064	0.38	4.992	0.34	0.019	0.041	0.004	<d.l.
CH0805_07	0.44	0.12	0.23	0.70	1.79	0.69	0.21	4.64	0.18	0.04	21.70	I < d.l.	25.97	4.95	0.022	0.038	1.21	5.072	0.28	0.001	0.036	0.003	<d.l.
CH0805_10	0.52	0.12	0.29	2.21	1.13	0.59	0.50	7.90	1.01	0.13	15.91	0.040	27.52	26.80	0.037		2.28	0.641	6.45	0.026	0.027	0.002	<d.l.
CH0805_12	0.44	0.11	0.65	2.47	2.83	0.38	1.29	8.84	1.12	0.13	6.84	0.007	54.56	6.67	0.060	0.132	0.57	2.102	0.75	0.007	0.029	0.002	<d.l.
CH0805_13	0.54	0.10	0.65	3.24	2.39	0.46	0.51	7.78	1.38	0.18	15.16	0.027	59.56	7.58	0.050	0.154	0.88	3.054	2.21	0.016	0.025	0.004	0.005
CH0805_14	n.a.	0.00	0.20	0.79	1.52	0.42	0.36	3.87	0.12	0.03	10.84	n.a.	n.a.	n.a.	n.a.	n.a.	n.a.	n.a.	n.a.	n.a.	n.a.	n.a.	n.a.
CH0805_19	n.a.	0.00	0.16	1.01	1.30	0.28	1.06	2.95	0.60	0.20	2.78	n.a.	n.a.	n.a.	n.a.	n.a.	n.a.	n.a.	n.a.	n.a.	n.a.	n.a.	n.a.
CH0805_26	0.15	0.02	0.22	1.03	2.37	0.90	0.83	3.28	0.81	0.25	3.97	0.011	24.96	2.12	0.019	0.036	0.23	0.700	2.49		0.009	0.001	<d.l.
CH0805_27	0.39	0.09	0.39	1.60	2.22	0.37	0.79	5.11	0.67	0.13	6.47	0.010	41.54	8.66	0.079	0.070	0.70	3.111	2.95	0.020	0.012	0.003	0.009
Phases 1 and 2																							
CH0805_03	0.30	0.08	0.45	1.09	2.43	0.38	0.25	6.79	0.17	0.02	27.40	<d.l.	40.76	2.80	0.043	0.087	0.55	8.011	0.32	0.013	0.076	0.002	<d.l.
CH0805_08	0.30	0.02	0.42	1.13	1.18	0.45	0.60	3.16	0.64	0.20	5.25	0.001	17.48	4.24	0.043	0.055	0.82	<d.l.	12.85	0.023	0.030	<d.l.	<d.l.
CH0805_15	0.55	0.13	0.60	3.04	3.87	0.59	0.60	9.30	2.17	0.23	15.56	0.004	24.20	11.87	0.021	0.092	0.24	2.677	4.86	0.027	0.024	0.002	<d.l.
CH0805_16	0.29	0.06	0.73	2.70	2.18	1.38	1.29	7.43	0.88	0.12	5.74	0.004	22.39	5.85	0.020	0.063	0.48	0.249	5.79	0.018	0.025	0.000	0.003
CH0805_29	0.37	0.02	0.52	1.01	1.19	0.37	0.65	2.94	0.48	0.16	4.54	<d.l.	8.84	5.99	0.041	0.106	1.43	0.606	5.74	0.001	10.008	0.002	<d.l.

na.: not analysed; d.l.: detection limit.
* Sample may include 5–6 May ashfall

Table 4
Mass element ratios in the Chaitén ash leachates measured in this study, and as reported in Martin et al. (2009).

Mass ratio	This study	Martin et al. (2009)
K:Cl	0.09	0.65
Cu:Cl	2×10^{-4}	2×10^{-4}
Cu:Ni	8.8	0.5
Cu:As	0.12	0.07
Cu:Cd	193	117
Cu:Zn	0.23	0.04
Cu:Fe	0.10	0.06
Cu:Mn	0.03	0.12

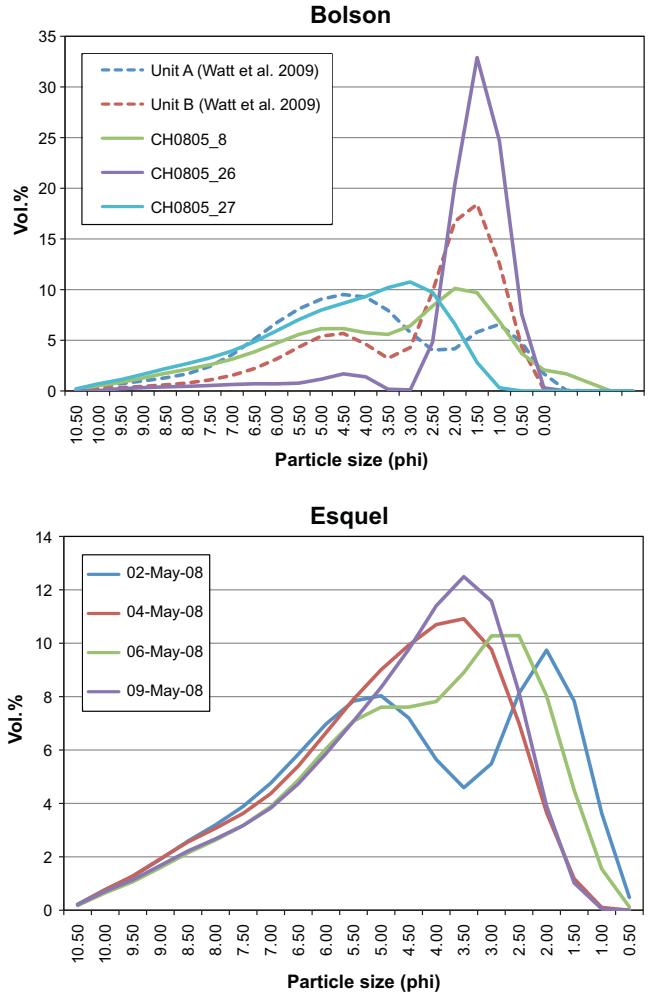

Fig. 11. Top: There were at least three fall units identified at El Bolson, Argentina (CH0805_26, CH0805_27, and CH0805_8, collected on 6, 7, and 8 May, respectively). These are compared to samples collected by Watt et al. (2009) in the same vicinity; bottom: there were also at least four discrete fall units identified through systematic sequential sampling at Esquel, Argentina (CH0805_4, CH0805_5, CH0805_6 and CH0805_7, collected on 2, 4, 6, and 9 May, respectively).

4.3. Propensity of ash aggregation through sedimentological fingerprinting

Fine ash was observed to form aggregates during most sedimentation events that resembled "snowflakes" (particle clusters, PC1; Brown et al., this issue). Ash particle clusters were identified in fallout in samples CH0805_24 and CH0805_23 (Fig. 8), and small pellets were observed *in situ* in several other deposits. The size of individual clusters was challenging to determine as individual aggregates broke up on deposition and measured between 0.5 and 2 mm diameter. Ash fallout was also accompanied by several brief periods of precipitation during the first week of the eruption, and in some cases the ash-fall was wet, as was the case of some of the samples collected on 4 May 2008 (Table 2).

The May 2008 Chaitén deposit was extremely fine grained even at distances ~100 km from the volcano. While there was greater variability in mean particle size closer to source, the lower end of the range of mean particle size converged on a value between 20 and 40 microns at most distances up to >500 km. The data are also compared to analysis of ash fallout from the Mount St. Helens 18 May 1980 eruption (Fig. 9) which was analysed using the same instrument (Durant et al., 2009). This earlier eruption injected volcanic particulates high into the upper troposphere/lower stratosphere and transport was dominantly in the westerly jet to the east of the volcano. In both cases, beyond some distance (100s km from the volcano), mean particle size became remarkably consistent and invariant.

There were five particle size subpopulations identified in May 2008 Chaitén fallout between ~80 and 250 km from the volcano, which decreased to three fine subpopulations between ~250 and 500 km from the volcano (Fig. 10). A similar pattern in the number and abundance of particle size subpopulations was observed in the Mount St. Helens distal ash deposit. There were abundant observations of particle aggregate fallout from the Mount St. Helens eruption cloud and the fine, invariant, mean particle size, and particle size subpopulations in fallout were linked to the aggregation process (Durant et al., 2009). The additional coarse subpopulation present closer to the volcano represents single particle settling. Based on observations of aggregate fallout and the similarity of the sedimentological characteristics, aggregation clearly played an important role in removal of fine ash erupted during the Chaitén eruption and in the spatial distribution of the resulting ash deposit.

4.4. Chemical leachates from eruption fallout and environmental implications

The 2008 eruption of Chaitén presented an opportunity to study transport of chemical species to local environments by rhyolitic ash fallout. It is generally accepted that experimentally-derived ash leachate compositions reflect the dissolution of water-soluble compounds, including sulphate, halide salts and acids adsorbed at the surfaces of the ash particles (Hinkley and Smith, 1982; Rose, 1977). The origin of these adsorbed compounds is ascribed to gas/aerosol-ash interaction within the volcanic eruption plume, and later within the volcanic cloud (Delmelle et al., 2007; Óskarsson, 1980; Rose, 1977). The near-neutral pH values and the relatively good charge balance of the experimentally-derived leachates indicate minimal quantities of acids were adsorbed onto ash particle surfaces.

The precise composition of the surface salts on ash is not directly measured but previous studies inferred stochiometries in ash leachates consistent with the dissolution of $CaSO_4$ and NaCl deposits (de Hoog et al., 2001; de Moor et al., 2005; Hinkley and Smith, 1982). Since Ca was present in excess of SO_4 in most of the leachates (Fig. 12a), it is likely that additional soluble Ca-bearing salts were present at the surface of the Chaitén ash. Sodium may be dominantly associated with Cl, but the Cl^- surplus points towards the existence of other chloride salts (Fig. 12b). XPS results provide further insights into the composition of the surface salts. The binding energy measured from the XPS Cl_{2p} (~198.6 eV) peak in CH0805_33 and CH0805_34 is consistent with Cl in NaCl, KCl, $FeCl_2$ and/or $CaCl_2$ (Wagner et al., 2010). Similarly, the XPS F_{1s} peak (~685.6 eV) may reflect F in NaF, CaF_2, KF, FeF_2 and/or FeF_3. Finally, a plot of the surface versus bulk composition for CH0805_33 and CH0805_34 revealed surface enrichments in Ca, Na and Fe

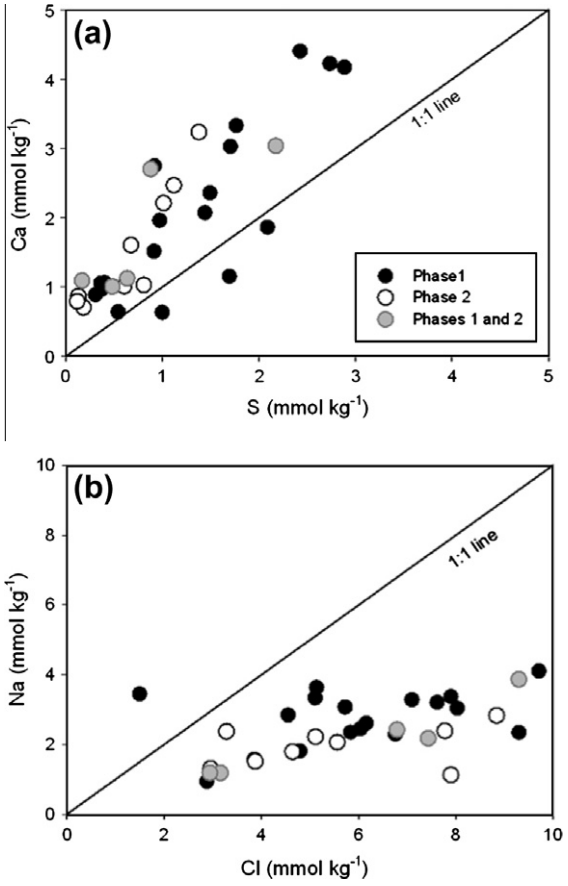

Fig. 12. Water-soluble Ca versus water-soluble S (A), and water-soluble Na versus water-soluble Cl (B) of the Chaitén ash leachates. See Table 3 for dataset.

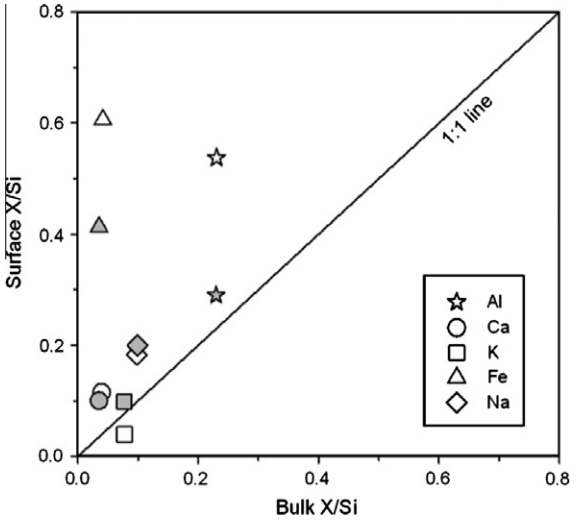

Fig. 13. Surface versus bulk compositions (normalised to Si) of the CH0805_32 and CH0805_33 ash samples from Chaitén.

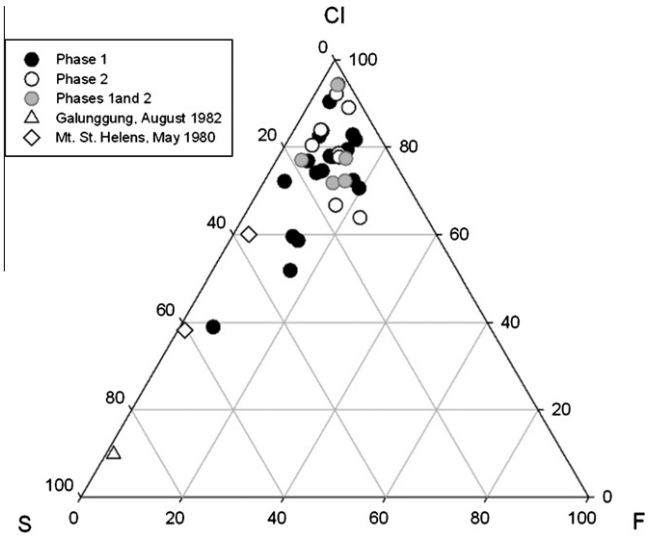

Fig. 14. Relative concentrations of water-soluble F, Cl and S of the ash leachates from Chaitén (circles). See Table 3 for dataset. Average compositions of ash leachates from the May 1980 eruption of Mount St. Helens volcano (Hinkley and Smith, 1982) and from the August 1982 eruption of Galunggung volcano (de Hoog et al., 2001) are shown for comparison.

(Fig. 13), suggesting the presence of coatings of mixed Ca-, Na- and Fe-rich salts. The origin of high Al concentrations measured at the surface of CH0805_32 is not immediately clear.

When compared to the average leachate composition of the distal ash from the 1980 eruption of Mount St. Helens (Hinkley and Smith, 1982), Chaitén ash leachates were about 4–6 times less concentrated. This may be attributed to a range of volcanic and environmental factors including contact duration between the ash and the eruptive gas phase, ash-to-gas ratio, ash composition, plume humidity (Óskarsson, 1980; Rose, 1977). We also speculate that higher leachate concentrates may result from higher ash particle specific surface area (SSA), although this quantity was challenging to measure using gas adsorption as ash sample masses were extremely small and the corresponding measurement errors large.

Several authors have used the S:Cl ratio measured in ash leachates to infer the composition of the eruptive gas phase. Except in one sample, the molar S:Cl ratio in the Chaitén ash leachates was consistently less than one, a value lower than that found for ash from other explosive magmatic eruptions, such as Mount St. Helens 1980 and Galunggung (Indonesia) 1982 eruptions (Fig. 14). For comparison, high temperature magmatic gases associated with subduction zones typically display a S:Cl ratio in the range ~2–8 (Giggenbach, 1996). Thus, the low S:Cl ratio values of the Chaitén ash leachates may reflect a relatively S-poor eruptive gas composition, in agreement with satellite observations (Carn et al., 2009) as well as with recent petrological estimates (Lowenstern et al., 2010). Similarly, the high Cl:F ratio values obtained for the ash leachates may suggest gas–ash interaction within a Cl-rich plume. Of note, the ash materials erupted during the 2–5 May and 6–9 May 2008 phases did not produce distinguishable S:Cl and Cl:F ratios (Table 3).

Based on field examination of the ash-fall deposits over Argentina, Watt et al. (2009) estimated that the total mass of ash erupted during the first of week of Chaitén explosive eruption in May 2008 was $\sim 1.7 \times 10^{11}$ kg. Assuming that this value represents a minimum mass of magma erupted over this period, and knowing that the pre-eruptive magmatic S content was less that 50 mg S kg^{-1} (Lowenstern et al., 2010), the total mass of S which may have been released during explosive degassing was $\sim 8.5 \times 10^6$ kg. Using an average S concentration in the ash leachate of ~1.1 mmol kg^{-1} of ash (or ~34 mg S kg^{-1} of ash), the total amount of S scavenged and returned to the Earth's surface via ash deposition was estimated to $\sim 5.8 \times 10^6$ kg (or ~68% of the S initially released) with the rest of the S ($\sim 2.7 \times 10^6$ kg) remaining in the gaseous

and aerosol phases. According to satellite measurements, $\sim 5 \times 10^6$ kg of S were emitted in Chaitén eruptive plumes on 2, 6 and 8 May 2008 (Carn et al., 2009). This figure is in reasonable agreement with that derived above, but a perfect match between the calculated and observed quantities of S injected into the atmosphere is obtained by using a lower average S concentration (i.e., 0.65 mmol kg^{-1} of ash) for the ash leachate. In this case, scavenging by ash would account for ~42% of the magmatic S release, a fraction comparable to those derived for explosive eruptions elsewhere (de Hoog et al., 2001; de Moor et al., 2005; Rose, 1977; Varekamp et al., 1984).

Deposition of volcanic ash onto terrestrial and aquatic ecosystems may lead to various physical, chemical and biological effects (Witham et al., 2005; and references therein). Data collected in June 2008 and January 2009 in the area impacted by Chaitén ash led Martin et al. (2009) to argue that ephemeral lakes which received more than 2 mm of ash were subject to compositional changes. This suggestion was based on the positive correlations between the concentrations of certain elements (Rb, Tl, K, As, Cs, Mn, Zn, Cl, Cd, Fe, B, Cu and Ni) and thickness of ash deposited in the five lakes surveyed. The underlying assumption was that Ca served as a reference element to account for the differences in dilution between the lakes; that is, the lake Ca concentration was not influenced by the entry of ash. This hypothesis is however challenged by our ash leachate measurements (Table 3). By considering these along with the ash thickness and lake morphometric data presented in Martin et al. (2009), we calculated that three ephemeral lakes probably received an input of ash-derived Ca corresponding to at least ~20% of the total dissolved Ca in the lake water. Martin et al. also derived elemental ratios in the soluble material adhering to the ash based on the lake chemical analyses (Table 3 in Martin et al. (2009)). However, comparison of these values with those measured in the ash leachates (Table 4) revealed significant discrepancies, possibly attributable to higher lake K, Ni, Zn, Fe and Mn concentrations that could be generated from ash leaching only. This suggests that beside ash deposition, other environmental factors need to be considered in order to explain the reported variability in the ephemeral lake compositions.

The lake locations reported in Martin et al. were revisited as part of the current study and it was noted that whereas the water bodies in Martin et al. were reported as "ephemeral lakes", a number of these water bodies were in fact "mallines" (wetlands) which are surface expressions of the local subsurface hydrological system. Usually these features develop in areas of active drainage systems with low relief and are linked closely to the water table. As there are fluxes in and out of these water bodies via the groundwater system, complications arise because the original water composition is not known. It is therefore challenging to assess the impact of leachates from ash fallout without information on the original water chemistry of a given water body, which would require a long time series of measurements to characterise any natural variability.

XPS analyses revealed that the ash surfaces of CH0805_33 and CH0805_34 were strongly enriched in Fe (Fig. 13). This result contrasts with the systematic depletion of surface Fe reported previously in various ash specimens (Delmelle et al., 2007), although the reason for this difference has not yet been established. The high value of Fe in the ash surface is not reflected in the leachate analyses; that is, the concentrations compare to those observed in other ash leachate studies (Witham et al., 2005). However, recent detailed measurements of the potential for Fe release in seawater for various ash samples indicate above-average values for the Chaitén ash (Olgun et al., in press), which may reflect the Fe enrichment detected at the ash particle surfaces. Furthermore, Fe at the ash surface may become readily mobilised on exposure to low pH values, for example when the ash is subject to cloud processing in the atmosphere (see Ayris and Delmelle, this issue).

These points are significant when considering the impact of ash deposition on ocean biogeochemical cycles. Our results indicate that the low Fe concentration measured in the ash leachate is unlikely to be a good indicator for inferring the potential of ash to act as a source of soluble Fe in the ocean. First, the amount of Fe needed to enhance phytoplankton is low anyway (see Duggen et al. 2009). Second, the ash leachate method is not designed to reproduce the seawater environment (see Duggen et al. (2009) and Olgun et al. (in press)). Iron is poorly soluble at near-neutral pH values (such as those observed in the experimentally-derived ash leachates) and dissolved Fe concentration is controlled by Fe (oxy)hydroxide precipitation (Stumm and Furrer, 1987). Thus there is high potential for Fe release following wet deposition of ash over the ocean. Therefore, we argue that the Fe release potential of the Chaitén ash should not be dismissed solely on the basis of its total Fe content (e.g., as suggested by Watt et al., 2009).

5. Conclusions

MODIS infrared ash particle retrievals and surface reflectance measurements show good spatiotemporal correspondence between observed cloud trajectories and increased surface reflectance inferred to indicate ash fallout. At any one moment during the period 3–7 May 2008 there was between 0.2 and 0.4 Tg of airborne ash <30 μm diameter suspended in the atmosphere. The ash deposit formed by the Chaitén eruption was dominated by fine grained and very fine grained angular rhyolitic glass shard particles up to a distance >500 km from the volcano. Particle size varied very little beyond a distance of about 300 km, and the extent of ash-fall continued and thinned to near zero to reach the east coast of the continent. It is inferred that fallout of fine ash from the Chaitén eruption cloud was dominantly driven by the formation of aggregates, perhaps aided by association with icy hydrometeors. Bulk ash leachate and XPS analyses revealed surface enrichments in Ca, Na and Fe, which suggests the presence of coatings of mixed Ca-, Na- and Fe-rich salts on ash particle surfaces prior to deposition. The low S:Cl ratios in Chaitén ash leachates may reflect a relatively S-poor eruptive gas composition, and high Cl:F ratios suggest gas–ash interaction within a Cl-rich plume. It is estimated that ash fallout had potential to scavenge ~42% of total S released into the atmosphere by the eruption. Furthermore, our results suggest that there may be a pool of Fe at the surface of ash particle surfaces that becomes available after exposure to low pH environments typical of volcanic plumes and clouds. It is possible, therefore, that the Fe release potential of Chaitén ash fallout over oceans could have been high enough to effect ocean productivity. It follows that bulk leachate analyses are unlikely to be a good indicator of the potential of ash to act as a source of soluble Fe in the ocean.

Acknowledgements

AJD gratefully acknowledges support from the Natural Environmental Research Council. Field work was supported by a CONICET special grant. We especially thank the Administración de Parques Nacionales, INTA, Municipalidad de Esquel, Dirección de Bosques de Chubut for their participation in the ash collection network. We also thank Valeria Outes at Centro Atómico Bariloche facility for providing SEM images of ash fallout. Sebastien Watt, Tamsin Mather and David Pyle are acknowledged and thanked for generously allowing access to their data, discussion on the sedimentology of the deposit, and assistance generating the fallout map. Marcelo Marquez and Nilda Menegatti from Universidad de la Patagonia San Juan Bosco supplied key distal samples and Claire Horwell kindly supplied three ash samples.

References

Alfano, F., Bonadonna, C., Volentik, A., Connor, C., Watt, S., Pyle, D., Connor, L., 2010. Tephra stratigraphy and eruptive volume of the May, 2008, Chaitén eruption. Chile. Bull. Volcanol., 1–18.

Blott, S.J., Wilson, H.E., Croft, D.J., Pye, K., Saye, S.E., 2004. Particle size analysis by laser diffraction. Geol. Soc. Spec. Publ. 232, 63–73.

Cakmur, R.V., Miller, R.L., Perlwitz, J., Geogdzhayev, I.V., Ginoux, P., Koch, D., Kohfeld, K.E., Tegen, I., Zender, C.S., 2006. Constraining the magnitude of the global dust cycle by minimizing the difference between a model and observations. J. Geophys. Res.-Atmos. 111. doi:10.1029/2005JD005791.

Carn, S.A., Pallister, J.S., Lara, L., Ewert, J.W., Watt, S., Prata, A.J., Thomas, R.J., Villarosa, G., 2009. The unexpected awakening of Chaitén volcano, Chile. Eos Trans. AGU 90. doi:10.1029/2009EO240001.

Castro, J.M., Dingwell, D.B., 2009. Rapid ascent of rhyolitic magma at Chaiten volcano, Chile. Nature 461, 780–783.

Dartevelle, S., Ernst, G.G.J., Bernard, A., 2002. Origin of the Mount Pinatubo climactic eruption cloud: Implications for volcanic hazards and atmospheric impacts. Geology 30, 663–666.

de Hoog, J.C.M., Koetsier, G.W., Bronto, S., Sriwana, T., van Bergen, M.J., 2001. Sulfur and chlorine degassing from primitive arc magmas: temporal changes during the 1982–1983 eruptions of Galunggung (West Java, Indonesia). J. Volcanol. Geotherm. Res. 108, 55–83.

de Moor, J.M., Fischer, T.P., Hilton, D.R., Hauri, E., Jaffe, L.A., Camacho, J.T., 2005. Degassing at Anatahan volcano during the May 2003 eruption: implications from petrology, ash leachates, and SO_2 emissions. J. Volcanol. Geotherm. Res. 146, 117–138.

Deligne, N.I., Coles, S.G., Sparks, R.S.J., 2010. Recurrence rates of large explosive volcanic eruptions. J. Geophys. Res. 115, B06203. doi:10.1029/2009JB006554.

Delmelle, P., Lambert, M., Dufrîne, Y., Gerin, P., Oskarsson, N., 2007. Gas/aerosol-ash interaction in volcanic plumes: new insights from surface analyses of fine ash particles. Earth Planet. Sci. Lett. 259, 159–170.

Duggen, S., Olgun, N., Croot, P., Hoffmann, L., Dietze, H., Teschner, C., 2009. The role of airborne volcanic ash for the surface ocean biogeochemical iron-cycle: a review. Biogeosci. Discuss. 6, 6441–6489.

Durant, A.J., Bonadonna, C., Horwell, C.J., 2010. Atmospheric and environmental impacts of volcanic particulates. Elements 6, 235–240.

Durant, A.J., Rose, W.I., Sarna-Wojcicki, A.M., Carey, S., Volentik, A.C.M., 2009. Hydrometeor-enhanced tephra sedimentation: constraints from the 18 May 1980 eruption of Mount St. Helens. J. Geophys. Res. – Sol Ea 114. doi:10.1029/2008JB005756.

Folch, A., Jorba, O., Viramonte, J., 2008. Volcanic ash forecast – application to the May 2008 Chaiten eruption. Nat. Hazards Earth Syst. Sci. 8, 927–940.

Gangale, G., Prata, A.J., Clarisse, L., 2010. The infrared spectral signature of volcanic ash determined from high-spectral resolution satellite measurements. Remote Sens. Environ. 114, 414–425.

Giggenbach, W.F., 1996. Chemical composition of volcanic gases. In: Tilling, R.S. (Ed.), Monitoring and Mitigation of Volcano Hazards. Springer-Verlag, Berlin Heidelberg, pp. 221–256.

Hinkley, T.K., Smith, K.S., 1982. Leachate Chemistry of Ash from the May 18, 1980 Eruption of Mount. St. Helens. US Geol. Survey Prof. Paper 1397-B, pp. 27–64.

Horwell, C.J., 2007. Grain-size analysis of volcanic ash for the rapid assessment of respiratory health hazard. J. Environ. Monit. 9, 1107–1115, doi: 1110.1039/b710583.

Horwell, C.J., Brana, L.P., Sparks, R.S.J., Murphy, M.D., Hards, V.L., 2001. A geochemical investigation of fragmentation and physical fractionation in pyroclastic flows from the Soufriere Hills volcano, Montserrat. J. Volcanol. Geotherm. Res. 109, 247–262.

Iglesias, V., Whitlock, C.L., Bianchi, M.M., 2011. Holocene Climate Variability and Environmental History at the Patagonian Forest/Steppe Ecotone: Lago Mosquito (lat. 42.50°S, long. 71.40°W) and Laguna del Cóndor (lat. 42.20°S, long. 71.17°W). Holocene, Sub Judice.

Kueppers, U., Perugini, D., Dingwell, D.B., 2006. "Explosive energy" during volcanic eruptions from fractal analysis of pyroclasts. Earth Planet. Sci. Lett. 248, 800–807.

Lara, L., 2009. The 2008 eruption of the Chaitén Volcano, Chile: a preliminary report. Andean Geol. 36, 125–129.

Lowenstern, J.B., Bleick, H., Castro, J.M., Pallister, J.S., Eichelberger, J.C., 2010. Halogen Degassing During Emplacement and Crystallisation of the Chaitén Rhyolitic Lava Dome(s), Abstract V34B-07 Presented at 2010 Fall Meeting, AGU, San Francisco, Calif., 13–17 December. American Geophysical Union, San Francisco.

Martin, R.S., Watt, S.F.L., Pyle, D.M., Mather, T.A., Matthews, N.E., Georg, R.B., Day, J.A., Fairhead, T., Witt, M.L.I., Quayle, B.M., 2009. Environmental effects of ashfall in Argentina from the 2008 Chaitén volcanic eruption. J. Volcanol. Geotherm. Res. 184, 462–472.

Mastin, L.G., 2007. Generation of fine hydromagmatic ash by growth and disintegration of glassy rinds. J. Geophys. Res.-Sol Ea 112. doi:10.1029/2005JB003883.

Mastin, L.G., Guffanti, M., Servranckx, R., Webley, P., Barsotti, S., Dean, K., Durant, A., Ewert, J.W., Neri, A., Rose, W.I., Schneider, D., Siebert, L., Stunder, B., Swanson, G., Tupper, A., Volentik, A., Waythomas, C.F., 2009. A multidisciplinary effort to assign realistic source parameters to models of volcanic ash-cloud transport and dispersion during eruptions. J. Volcanol. Geotherm. Res. 186, 10–21.

Naranjo, J.A., Stern, C.R., 2004. Holocene tephrochronology of the southernmost part (42°30'–45°S) of the Andean Southern Volcanic Zone. Rev. Geol. Chile 31, 225–240.

Olgun, N., Duggen, S., Croot, P.L., Delmelle, P., Dietze, H., Schacht, U., Óskarsson, N., Siebe, C., Auer, A., Garbe-Schönberg, 2011. Surface ocean iron fertilization: the role of airborne volcanic ash from subduction zone and hotspot volcanoes and related iron-fluxes into the Pacific Ocean. Global Biogeochem. Cycles, doi:10.1029/2009GB003761, in press.

Óskarsson, N., 1980. The interaction between volcanic gases and tephra: fluorine adhering to tephra of the 1970 Hekla eruption. J. Volcanol. Geotherm. Res. 8, 251–266.

Pallister, J.S., Major, J.J., Pierson, T.C., Hoblitt, R.P., Lowenstern, J.B., Eichelberger, J.C., Lara, L., Moreno, H., Munoz, J., Castro, J.M., Iroume, A., Andreoli, A., Jones, J., Swanson, F., Crisafulli, C., 2010. Interdisciplinary studies of eruption at Chaiten volcano, Chile. EOS Trans. AGU 91, 381–382.

Pollack, J.B., Toon, O.B., Khare, B.N., 1973. Optical properties of some terrestrial rocks and glasses. Icarus 19, 372–389.

Prata, A.J., Grant, I.F., 2001. Retrieval of microphysical and morphological properties of volcanic ash plumes from satellite data: application to Mt Ruapehu, New Zealand. Quart. J. Roy. Meteor. Soc. 127, 2153–2179.

Pyle, D.M., 2000. Sizes of volcanic eruptions. In: Sigurdsson, H., Houghton, B.F., McNutt, S.R., Rymer, H., Stix, J. (Eds.), Encyclopedia of Volcanoes. Academic Press, London, UK, pp. 263–269.

Rose, W.I., 1977. Scavenging of volcanic aerosol by ash: atmospheric and volcanologic implications. Geology 5, 621–624.

Rose, W.I., Durant, A.J., 2009. Fine ash content of explosive eruptions. J. Volcanol. Geotherm. Res. 186, 32–39.

Rose, W.I., Riley, C.M., Dartevelle, S., 2003. Sizes and shapes of 10-Ma distal fall pyroclasts in the Ogallala group, Nebraska. J. Geol. 111, 115–124.

Scasso, R.A., Corbella, H., Tiberi, P., 1994. Sedimentological analysis of the tephra from the 12–15 August 1991 eruption of Hudson Volcano. Bull. Volcanol. 56, 121–132.

Simkin, T., Siebert, L., 2002. Global Volcanism FAQs. Smithsonian Institution, Global Volcanism Program Digital Information Series GVP-5. <http://www.volcano.si.edu/faq/>.

Stumm, W., Furrer, G., 1987. The dissolution of oxides and aluminum silicates; examples of surface-coordination-controlled kinetics. In: Stumm, W. (Ed.), Aquatic Surface Chemistry: Chemical Processes at the Particle-Water Interface. Wiley-Interscience, New York.

Thomason, L.W., Pitts, M.C., 2008. CALIPSO observations of volcanic aerosol in the stratosphere. In: Upendra N.S., Kazuhiro A., Achuthan J. (Eds.), Lidar Remote Sensing for Environmental Monitoring IX. Society of Photo-Optical Instrumentation Engineers, Bellingham, WA, USA, pp. 71530O–71530O–71538.

Tuffen, H., Smith, R., Sammonds, P.R., 2008. Evidence for seismogenic fracture of silicic magma. Nature 453, 511–514.

Varekamp, J.C., Luhr, J.F., Prestegaard, K.L., 1984. The 1982 eruptions of El Chichón Volcano (Chiapas, Mexico), character of the eruptions, ash-fall deposits, and gas phase. J. Volcanol. Geotherm. Res. 23, 39–68.

Wagner, C.D., Naumkin, K.V., Kraut-Vass, A., Allison, J.W., Powell, C.J., Rumble, J.R., 2010. NIST X-ray Photoelectron Spectroscopy Database, Version 3.5, National Institute of Standards.

Watt, S.F.L., Pyle, D.M., Mather, T.A., Martin, R.S., Matthews, N.E., 2009. Fallout and distribution of volcanic ash over Argentina following the May 2008 explosive eruption of Chaiten, Chile. J. Geophys. Res.-Sol Ea 114, B04207. doi:10.1029/2008JB006219, 002009.

Wen, S., Rose, W.I., 1994. Retrieval of sizes and total masses of particles in volcanic clouds using AVHRR bands 4 and 5. J. Geophys. Res. 99, 5421–5431.

Wilson, T.M., Leonard, G.S., Stewart, C., Baxter, P.J., Villarosa, G., Rovere, E.I., Johnston, D., Cronin, S.J., 2009a. Impacts on agriculture following the May 2008 Chaitén eruption in Patagonia. Geol. Soc. Am. Abstr. Programs 41, Paper No. 189–182.

Wilson, T.M., Leonard, G.S., Stewart, C., Villarosa, G., Rovere, E.I., Baxter, P.J., Johnston, D., Cronin, S.J., 2009b. Impacts on critical infrastructure following the May 2008 Chaitén eruption in Patagonia. Geol. Soc. Am. Abstr. Programs 41, Paper No. 164–110.

Witham, C.S., Oppenheimer, C., Horwell, C.J., 2005. Volcanic ash-leachates: a review and recommendations for sampling methods. J. Volcanol. Geotherm. Res. 141, 299–326.

Wohletz, K.H., 1983. Mechanisms of hydrovolcanic pyroclast formation: grain-size, scanning electron microscopy, and experimental studies. J. Volcanol. Geotherm. Res. 17, 31–63.

Wohletz, K.H., Sheridan, M.F., Brown, W.K., 1989. Particle-size distributions and the sequential fragmentation transport-theory applied to volcanic ash. J. Geophys. Res.-Sol. Ea. 94, 15703–15721.